

## Driven Front Propagation in 1D Spatially Periodic Media

F. Haudin,<sup>1</sup> R. G. Elías,<sup>2</sup> R. G. Rojas,<sup>3</sup> U. Bortolozzo,<sup>1</sup> M. G. Clerc,<sup>2</sup> and S. Residori<sup>1</sup>

<sup>1</sup>*INLN, Université de Nice Sophia-Antipolis, CNRS, 1361 route des Lucioles 06560 Valbonne, France*

<sup>2</sup>*Departamento de Física, FCFM, Universidad de Chile, Casilla 487-3, Santiago, Chile*

<sup>3</sup>*Instituto de Física, Pontificia Universidad Católica de Valparaíso, Casilla 4059, Valparaíso, Chile*

(Received 6 June 2009; published 18 September 2009)

We study front propagation in one-dimensional spatially periodic media. Based on an optical feedback with a spatially amplitude modulated beam, we set up a one-dimensional forced experiment in a nematic liquid crystal cell. By changing the forcing parameters, the front exhibits a pinning effect and oscillatory motion, which are confirmed by numerical simulations for the average liquid crystal tilt angle. A spatially forced dissipative  $\phi^4$  model, derived at the onset of bistability, accounts qualitatively for the observed dynamics.

DOI: 10.1103/PhysRevLett.103.128003

PACS numbers: 45.70.Qj, 05.45.-a, 47.54.-r

In nonequilibrium processes different extended states, developing from bifurcations or phase transitions, can coexist for the same values of parameters [1]. The coexistence is characterized by spatial domains, with interfaces, or *fronts*, propagating between them. Thus, before a system reaches an equilibrium state, the dynamics is characterized by a rich and complex interface evolution. The concept of front propagation, emerged in the context of populations dynamics [2], has attracted, since then, a growing interest in chemistry, physics and mathematics. In physics, fronts play a central role in a large variety of situations, ranging from reaction diffusion models, solidification processes, flame propagation, to pattern forming systems (see, e.g., [3,4] and references therein). From the point of view of dynamical systems theory in 1D spatial dimension, a front is a nonlinear solution described in phase space as a heteroclinic orbit linking two spatially extended states [5]. One of the most studied fronts is that connecting a stable uniform state with an unstable one, so called the FKPP-front [6], whose propagation speed is not unique and is fixed by the initial conditions [7]. Another well-known type of front, the normal front, connects two stable uniform states. The normal front appears inside the bistability region and is characterized by a unique speed that is given, if the system is variational, by the free energy difference between the two states [8]. Therefore, the most favorable state invades the less favorable one, and the front speed is zero only at the Maxwell point, for which both states have the same energy [9].

A fundamental issue in front dynamics is that of propagation over periodic media. As firstly pointed out by Pomeau [10], the presence of a spatial periodicity is expected to induce an energy barrier for the front propagation to occur, so that the front speed should become zero for a relatively large interval of parameters, so called the pinning range. The pinning range has been discussed in several physical contexts, such as pattern selection with different symmetries in generalized Swift-Hohenberg models, the crystallization kinetics of cellular patterns

and defect dynamics [11]. In the last two decades a lot of theoretical efforts have been devoted to the understanding of front dynamics inside and near the pinning range, where front interactions have been identified as responsible for the appearance of localized structures that are patterns extended over a limited space region [5,11–15]. However, despite the large number of theoretical and numerical studies, an experimental characterization of the pinning range and relative front dynamics is not yet available. In a bidimensional forced system, the anisotropy of the front velocity has been shown [16]; nevertheless, the issue of the existence of a pinning range was not addressed. Experimentally, this question has a fundamental relevance in numerous domains where front propagation is involved, for example, in fluids [17] or in chemical reactions [18] for the formation of nonlinear structures, in microfluidic chips [19] for the process of drop coalescence, in the wetting of microstructured surfaces [20], for controlling the motility of bacteria [21] or the growth of self-assembly monolayers [22].

In this Letter, we present what is, to our knowledge, the first experimental characterization of the pinning range and front propagation in 1D spatially periodic media. Based on an optical feedback with a spatially amplitude modulated input beam, we set up a 1D forced configuration in a nematic liquid crystal cell. In a large region of parameter space, the system exhibits fronts connecting two different average orientations of the liquid crystal molecules. By introducing the spatial forcing, the fronts exhibit a large pinning effect, as well as spatially oscillating motion outside the pinning region. Theoretically, we derive a spatially forced dissipative  $\phi^4$  model, which is valid close to the onset of bistability and accounts analytically for the observed dynamics. Numerical simulations of the average liquid crystal tilt angle  $\theta$  exhibit a dynamical behavior in good agreement with the experimental and analytical results.

The experimental setup, schematically represented in Fig. 1(a), comprises a liquid crystal light valve (LCLV)

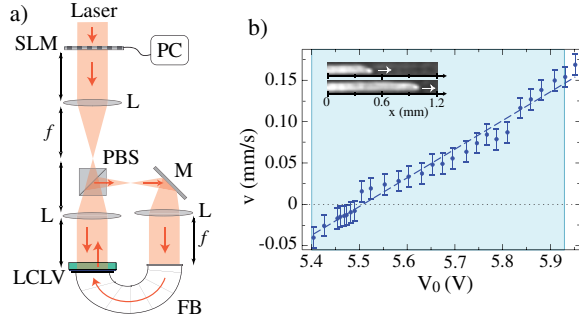


FIG. 1 (color online). (a) Schematic experimental setup. (b) Front velocity  $v$  against the voltage  $V_0$  in the unforced experiment; the blue shaded area is the bistable region, points are experimental data, the dashed line is a theoretical fit. In the inset: two successive snapshots (top  $t = 0$ , bottom  $t = 4$  s) of an expanding front.

with optical feedback. The LCLV is made of a thin nematic liquid crystal (LC) layer inserted in between a glass plate and a photoconductive wall over which a dielectric mirror is deposited. An externally applied  $V_0$  voltage induces an electric field in the direction into which molecules tend to orientate. When reflected by the mirror after passing through the LC layer, light gets a phase shift  $\Delta\varphi$  that is a function of the LC orientation angle, which, as we will see below, depends on the intensity  $I_w$  on the photoconductor. The input laser beam,  $\lambda = 632$  nm, is enlarged up to a diameter of 1 cm and collimated. A spatial light modulator (SLM) controls the intensity profile at the entrance of the feedback loop, which contains a polarizing beam splitter (PBS), a mirror (M) and is closed by a fiber bundle (FB). Three lenses (L) of the same  $f = 25$  cm focal length, and placed at focal distance from their respective cofocal planes, ensure a self-imaging configuration, for which the intensity distribution at the SLM is exactly imaged on the LCLV and the rear side of the FB and the front side of the LCLV are conjugate planes. By doing this, the diffraction length in the feedback loop is set to zero, a condition that, together with the polarization interference introduced by the PBS, enables us to have fronts between stable homogeneous states [23]. In the transverse plane, these states appear with different intensity levels, and fronts between them can easily be observed as “black or white” interfaces.

The SLM consists of a liquid crystal display, one inch diagonal size, with a  $1024 \times 768$  pixels, each coded in 8 bits of intensity level, and interfaced to a personal computer. By using a dedicated software, intensity masks are produced in order to control the front dynamics and impose a quasi-unidimensional spatially periodic forcing. A zero-level intensity is set everywhere except on a narrow channel of  $150 \mu\text{m}$  width and  $2.5$  mm length. In the channel, the intensity is set either to a uniform level  $A$  or spatially modulated with an amplitude  $B$  and wavelength  $p$ . The general expression for the input beam profile is  $I_{\text{in}}(x) = A + B \sin(2\pi x/p)$ , where both  $A$  and  $B$  can be controlled

by changing the transmittance of the SLM. In the set of measurements here presented we have fixed  $A = 0.9 \text{ mW/cm}^2$  and  $B = 0.1 \text{ mW/cm}^2$ . We first study the front dynamics of the unforced system. As the voltage  $V_0$  is varied as a control parameter, we identify the bistable region, where two different molecular orientation states coexist. In this region, the more stable state tends to invade all the available space, developing an expanding or retracting front. By recording with a CCD camera the interface evolution over the channel, we have measured the front speed  $v$ , which is plotted in Fig. 1(b) as a function of  $V_0$ . Two successive snapshots of an expanding front are shown in the inset. The front speed grows linearly with  $V_0$  and changes its sign at the Maxwell point. The front is motionless only at the Maxwell point while retracting, respectively, expanding on the left, right of this point, as expected from the theory [9].

The above scenario is drastically modified when the system is spatially forced, so that the uniform states transform into patterns. In this case, the front either propagates by periodical leaps or stays motionless in a large region of parameters. In Fig. 2(a) the average front velocity  $\langle v \rangle$  is plotted against  $V_0$  for a forcing wavelength  $p = 115 \mu\text{m}$ . We can note that a large pinning range exists, where the front propagation is characterized by periodical leaps. For larger values of  $V_0$  the front speed oscillates regularly. Three successive snapshots of an expanding spatially modulated front are shown in the inset of Fig. 2(a). Correspondingly, a transverse section of the front profile is displayed in Fig. 2(b). In Fig. 2(c) three spatio-temporal

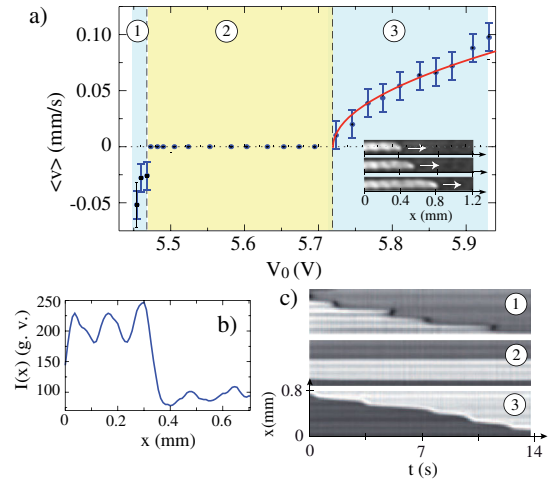


FIG. 2 (color online). (a) Average front velocity  $\langle v \rangle$  against the voltage  $V_0$  in the forced experiment,  $p = 115 \mu\text{m}$ ; the blue (dark gray) shaded area is the bistable region, the yellow (light gray) shaded area is the pinning range; the solid red line is Eq. (4) with  $\eta_+ = 5.72$ . In the inset: three successive snapshots (top  $t = 0$ , middle  $t = 3.2$ , bottom  $t = 6.4$  s) of an expanding front. (b) A typical transverse front profile; g.v. are gray values. (c) Space-time diagrams of the front evolution in regions 1, 2 and 3.

diagrams are shown, obtained from the front evolution in region 1, retracting front; region 2, the pinning range; and region 3, expanding front. As a consequence of the spatial forcing, the front is pinned over a large range of parameter, confirming the prediction of Pomeau [10] that an energy barrier has to exist when the front propagates over a spatially structured state.

The experimental behavior is confirmed by numerical simulations of the model for the LCLV with optical feedback, which consists in a relaxation equation for the average liquid crystal tilt angle  $\theta(x, t)$ ,  $0 \leq \theta \leq \pi/2$ , coupled with an equation for the feedback light intensity  $I_w$  [23,24]. In the case of zero diffraction length in the feedback loop, the equation for  $I_w$  can easily be solved, and the full LCLV model reads as

$$\tau_{LC} \partial_t \theta = l^2 \partial_{xx} \theta - \theta + \begin{cases} 0 & V_{LC} < V_{FT} \\ \frac{\pi}{2} (1 - \sqrt{\frac{V_{FT}}{V_{LC}(\theta)}}) & V_{LC} \geq V_{FT} \end{cases} \quad (1)$$

where  $x$  is the transverse direction of the LC layer,  $\tau_{LC} = 30$  ms the LC relaxation time,  $l = 30 \mu\text{m}$  the electric coherence length and  $V_{LC}(\theta) \equiv \Gamma V_0 + \alpha I_w$  the effective voltage applied to the liquid crystals, with  $V_{FT} = 3.2 V_{\text{rms}}$  the threshold for the Fréedericksz transition,  $\Gamma \sim 0.3$  the overall impedance of the LCLV dielectric layers and  $\alpha \sim 5.5 \text{ V cm}^2/\text{mW}$  a phenomenological parameter summarizing, in the linear approximation, the response of the photoconductor. The light intensity reaching the photoconductor is  $I_w = I_{\text{in}}[1 + \cos(\Delta\varphi)]$ , where  $\Delta\varphi = \beta \cos^2 \theta$  is the overall phase shift experienced by the light traversing the LC layer,  $\beta = 2kd\Delta n$  with  $d = 15 \mu\text{m}$  the thickness of the nematic layer,  $\Delta n = 0.2$  the LC birefringence and  $k = 2\pi/\lambda$  with  $\lambda = 632.5 \text{ nm}$ .

For uniform  $I_{\text{in}}$  and by increasing  $V_0$ , the above model Eq. (1) exhibits several bistability branches and, in the bistability regions, the front solutions display a velocity increasing linearly with  $V_0$ , in agreement with the experimental observations for the unforced system. When we introduce a small spatial forcing,  $I_{\text{in}}(x) = [A + B \sin(2\pi x/p)]$ ,  $B \neq 0$ , the uniform equilibria become periodic states and numerical simulations of the front dynamics show a large pinning range as in the experiment. In Fig. 3 we report experimental and numerical spatio-temporal diagrams showing the front evolution in region 3, starting from a local initial condition and at different forcing wavelengths. In the simulations the forcing parameters are  $A = 1$ ,  $B = 0.2$  and the other parameters are set to the same values as in the experiment. When we increase the forcing wavelength  $p$ , the pinning range increases whereas the average front speed decreases. Moreover, the upper states show larger amplitude modulations, an effect that results from the nonlinear dependence of the spatial forcing in  $V_{LC}$  [25], and which appears also in the experiment [see Fig. 2(b)].

Close to the point of nascent bistability,  $I_{\text{in}} \equiv I_c$ ,  $V_0 \equiv V_c$  and  $\theta \equiv \theta_0$ , we can reduce the above model, Eq. (1), to

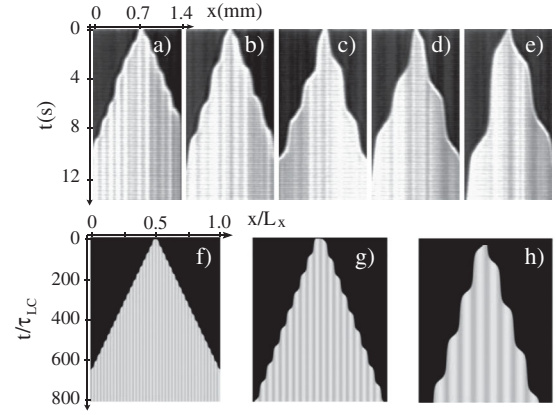


FIG. 3. Spatio-temporal plots of fronts propagating from a local initial condition at increasing forcing wavelength. Top: experiment,  $p =$  (a) 115, (b) 173, (c) 230, (d) 280, (e) 345  $\mu\text{m}$ . Bottom: numerical simulations,  $p =$  (f) 0.025, (g) 0.05, (h) 0.1  $L_x$ , with  $L_x = 800$  the number of integration points.

a forced dissipative  $\phi^4$  model, which reads as [26]

$$\tau \partial_t \phi = \eta + \varepsilon \phi - \phi^3 + l^2 \partial_{xx} \phi + (b + c \phi) \sin\left(\frac{2\pi x}{p}\right), \quad (2)$$

where  $\phi$  is the order parameter, which is related to the average director tilt by the expression  $\theta \approx \theta_0 + \phi/[2\beta \cos^2 \theta_0 \cot(\beta \cos^2 \theta_0) + (4 + \beta^2 \sin^2 \theta_0)/3 - 2/(\pi/2 - \theta_0)^2]^{1/2}$ . The unforced system ( $b = c = 0$ ) describes an imperfect extended pitchfork bifurcation [4] and has a motionless front solution at the Maxwell point,  $\eta = 0$ . This front, whose expression is  $\phi_k(x - x_0) = \pm \sqrt{\varepsilon} \tanh[\sqrt{\varepsilon} l^2/2(x - x_0)]$ , connects asymptotically the state  $\sqrt{\varepsilon}$  with  $-\sqrt{\varepsilon}$ . Close to the Maxwell point the front speed increases linearly with  $\eta$ , which is qualitatively consistent with the experimental behavior. When we introduce the spatial forcing ( $b \sim c \neq 0$ ), the uniform states become periodic with an amplitude proportional to  $B$  and a wavelength  $p$ . The front solution connecting the spatially periodic states exhibits a pinning range. Figure 4 and the inset depict the observed pinning range for the full LCLV model, Eq. (1), and for the  $\phi^4$  model, Eq. (2), respectively.

To study analytically the effect of the forcing, we consider the ansatz  $\phi(x, t) = \phi_k[x - x_0(t)] + w(x, x_0)$ , where  $x_0$  is the position of the front core. After straightforward calculations, we derive the solvability condition [27]

$$\dot{x}_0 = -\frac{3\eta}{\sqrt{2\varepsilon}} - \gamma(p) \sin\left(\frac{2\pi}{p} x_0 + \chi\right), \quad (3)$$

from which we see that the front speed has a constant term, first right-hand side, and a spatially oscillating part, second right-hand side, with  $\gamma(p) = 2\pi^2 \text{cosech}(\sqrt{2}\pi^2/p) \times \sqrt{9b^2 p^2 + 2c^2 \pi^2}/2p^3$  and  $\tan \chi = \sqrt{2}c\pi/3bp$ . The front is motionless in the range of parameters for which the first term is smaller than the amplitude of the periodic term,

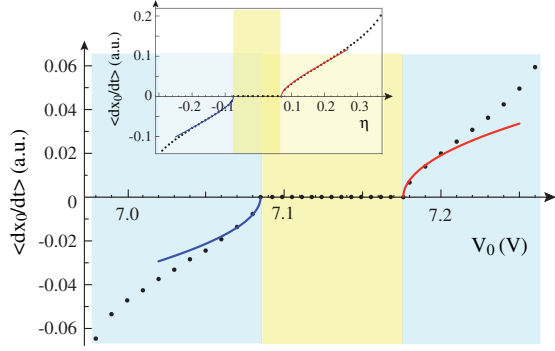


FIG. 4 (color online). Bifurcation structure of the average front speed  $\langle dx_0/dt \rangle$  for the full LCLV model, Eq. (1); a.u. are arbitrary units. In the inset, the average front speed for the  $\phi^4$  model, Eq. (2), is plotted against  $\eta$ . Points are numerical simulations, solid lines are theoretical fits with Eq. (4). The forcing parameters are  $A = 1$ ,  $B = 0.2$ ,  $p = 0.05 L_x$ .

which defines the pinning range  $\eta_- \leq \eta \leq \eta_+$ , the critical values being  $\eta_{\pm} \equiv \pm \sqrt{2\varepsilon\gamma(p)}/3$ . Outside this region, the front propagates with a spatially oscillating speed. In order to compute the average front speed we can integrate the above Eq. (3), and obtain  $x_0(t) = x_0(t_0) + p/2\pi \arctan[\tan(p/2\pi\sqrt{9\eta^2/\gamma^2 2\varepsilon - 1t})\sqrt{3\eta + \gamma\sqrt{2\varepsilon}/\sqrt{3\eta - \gamma\sqrt{2\varepsilon}}]$ . From this expression we derive the average front speed [27]

$$\left\langle \frac{dx_0}{dt} \right\rangle = \frac{3\sqrt{2}}{2} \eta \sqrt{1 - \left(\frac{\eta_{\pm}}{\eta}\right)^2}. \quad (4)$$

For  $|\eta| < |\eta_{\pm}|$  the above formula is imaginary, i.e., the front speed is zero, whereas close to  $\eta_{\pm}$ , it recovers the dynamical behavior expected for the pinning-depinning transition [28] (saddle-node bifurcation), with the front speed increasing as the square root of  $\eta$ ,  $\langle dx_0/dt \rangle \approx \pm 3\sqrt{(\eta - \eta_{\pm})\eta_{\pm}}$ . For large  $\eta$ , the average front speed behaves as a linear function of  $\eta$ . In Fig. 4,  $\langle dx_0/dt \rangle$  is plotted as a solid curve and compared with the numerical results for the full LCLV model, Eq. (1) and with the numerical results for the forced dissipative  $\phi^4$  model, Eq. (2) in the inset, respectively. We see, from comparison, that the  $\phi^4$  model is a qualitatively good description of the spatially driven front propagation and pinning effect.

In conclusion, we have shown the existence of a large pinning range and characterized the front dynamics in a LCLV experiment with spatially modulated optical feedback. Such an ability to control front propagation could be extended to other systems, thus opening the way to control front dynamics and localized states in structured or periodic media, as well as allowing the verification of several theoretical conjectures on front interactions, snaking bifurcations, and noise induced propagation.

M.G.C. acknowledges the FONDECYT Project No. 1090045, and FONDAP Grant No. 11980002. R.G.R. thanks the FONDECYT Project No. 11080286.

R.G.E. thanks the financial support Becas de Estadias Cortas de Investigaci3n de la Universidad de Chile. U.B. and S.R. thanks the ANR-07-BLAN-0246-03, turbonde.

- [1] G. Nicolis and I. Prigogine, *Self-Organization in Non-equilibrium Systems* (J. Wiley & Sons, New York, 1977).
- [2] R.A. Fisher, *Ann. Eugenics* **7**, 355 (1937); A. Kolmogorov, I. Petrovsky, and N. Piskunov, *Bull. Univ. Moskow Ser. Int. Sec. A* **1**, 1 (1937).
- [3] J. S. Langer, *Rev. Mod. Phys.* **52**, 1 (1980).
- [4] M. C. Cross and P. C. Hohenberg, *Rev. Mod. Phys.* **65**, 851 (1993).
- [5] W. van Saarloos and P.C. Hohenberg, *Physica (Amsterdam)* **56D**, 303 (1992).
- [6] P. Collet and J.P. Eckmann, *Instabilities and Fronts in Extended Systems* (Princeton University Press, Princeton, 1990).
- [7] W. van Saarloos, *Phys. Rep.* **386**, 29 (2003).
- [8] M. G. Clerc *et al.*, *Eur. Phys. J. D* **28**, 435 (2004).
- [9] R. E. Goldstein *et al.*, *Phys. Rev. A* **43**, 6700 (1991).
- [10] Y. Pomeau, *Physica (Amsterdam)* **23D**, 3 (1986).
- [11] See, e.g., L.M. Pismen, *Patterns and Interfaces in Dissipative Dynamics* (Springer Series in Synergetics, Berlin Heidelberg, 2006), and references therein.
- [12] P. Couillet, C. Riera, and C. Tresser, *Phys. Rev. Lett.* **84**, 3069 (2000).
- [13] M. Tiidi, Paul Mandel, and R. Lefever, *Phys. Rev. Lett.* **73**, 640 (1994).
- [14] M. G. Clerc and C. Falcon, *Physica (Amsterdam)* **356A**, 48 (2005).
- [15] J. Burke and E. Knobloch, *Phys. Rev. E* **73**, 056211 (2006).
- [16] J. Armero *et al.*, *Europhys. Lett.* **33**, 429 (1996); J. Armero *et al.*, *Phys. Rev. E* **56**, 5405 (1997).
- [17] T. Epstein and J. Fineberg, *Phys. Rev. Lett.* **92**, 244502 (2004).
- [18] V. Petrov, Q. Ouyang, and H.L. Swinney, *Nature (London)* **388**, 655 (1997).
- [19] A.R. Thiam, N. Bremond, and J. Bibette, *Phys. Rev. Lett.* **102**, 188304 (2009).
- [20] M. Sbragaglia *et al.*, *Phys. Rev. Lett.* **99**, 156001 (2007).
- [21] C. Douarche *et al.*, *Phys. Rev. Lett.* **102**, 198101 (2009).
- [22] J.F. Douglas *et al.*, *Proc. Natl. Acad. Sci. U.S.A.* **104**, 10 324 (2007).
- [23] S. Residori, *Phys. Rep.* **416**, 201 (2005).
- [24] M. G. Clerc, A. Petrossian, and S. Residori, *Phys. Rev. E* **71**, 015205(R) (2005).
- [25] U. Bortolozzo, M. G. Clerc, and S. Residori, *Phys. Rev. E* **78**, 036214 (2008).
- [26] The coefficients are  $\eta \equiv \frac{2\alpha}{\pi^2 V_{FT}} [1 - \cos(\beta \cos^2 \theta_0)] (\pi/2 - \theta_0)^3 [\Gamma_{I_{in}} - \Gamma_{I_c} + \alpha(1 - \cos(\beta \cos^2 \theta_0)(V_0 - V_c))]$ ,  $\varepsilon \equiv \frac{12}{\pi^2 V_{FT}} [(\pi/2 - \theta_0)^2 (V_0 - V_c)] + \frac{12}{\pi^2 V_{FT}} [(\frac{\pi^2 V_{FT}}{12} - (\pi/2 - \theta_0)^2)(I_{in} - I_c)/I_c]$ ,  $b \equiv \frac{2\alpha B}{\pi^2 V_{FT}} [1 - \cos(\beta \cos^2 \theta_0)] \times (\pi/2 - \theta_0)^3$ ,  $c \equiv \frac{B}{I_c} [1 - \frac{12V_0}{\pi^2 V_{FT}} (\pi/2 - \theta_0)^2]$ .
- [27] R. Rojas, Ph.D. thesis, University of Nice-Sophia Antipolis, 2005, <http://tel.archives-ouvertes.fr>.
- [28] N. Dirr and N. K. Yip, *Interfaces and Free Boundaries* **8**, 79 (2006).